Journal of Nuclear Materials 398 (2010) 87–92

Contents lists available at ScienceDirect

Journal of Nuclear Materials

journal homepage: www.elsevier.com/locate/jnucmat

Development of re-crystallized W–1.1%TiC with enhanced room-temperature ductility and radiation performance

H. Kurishita [a,*], S. Matsuo [a], H. Arakawa [a], T. Sakamoto [b], S. Kobayashi [b], K. Nakai [b], T. Takida [c], M. Kato [c], M. Kawai [d], N. Yoshida [e]

[a] International Research Center for Nuclear Materials Science, IMR, Tohoku University, Oarai, Ibaraki 311-1313, Japan
[b] Department of Materials Science and Biotechnology, Ehime University, Matsuyama 790-8577, Japan
[c] A.L.M.T. Corp., Toyama 931-8543, Japan
[d] Institute of Material Structure Science, High Energy Accelerator Research Organization (KEK), Tsukuba 305-0801, Japan
[e] Institute for Applied Mechanics, Kyushu University, Kasuga, Fukuoka 816-8580, Japan

A B S T R A C T

Ultra-fine grained (UFG) W–TiC compacts fabricated by powder metallurgical methods utilizing mechanical alloying (MA) are very promising for use in irradiation environments. However, the assurance of room-temperature ductility and enhancement in surface resistances to low-energy hydrogen irradiation are unsettled issues. As an approach to solution to these, microstructural modification by hot plastic working has been applied to UFG W–TiC processed by MA in a purified Ar or H_2 atmosphere and hot isostatic pressing (HIP). Hot plastically worked compacts have been subjected to 3-point bend tests at room temperature and TEM microstructural examinations. It is found that the microstructural modification allows us to convert UFG W–1.1%TiC to compacts exhibiting a very high fracture strength and appreciable ductility at room temperature. The compacts of W–1.1%TiC/Ar (MA atmosphere: Ar) and W–1.1%TiC/H_2 (MA atmosphere: H_2) exhibit re-crystallized structures with approximately 0.5 and 1.5 μm in grain size, respectively. It is shown that the enhancement of fracture resistance by microstructural modifications is attributed to significant strengthening of weak grain boundaries in the re-crystallized state. As a result the modified compacts exhibit superior surface resistance to low-energy deuteron irradiation.

1. Introduction

Tungsten (W), a refractory transition metal in group VIA, is extensively used as a spallation neutron source solid target [1] because of its large mass number, high density, good thermal conductivity, low thermal expansion coefficient, reduced radio activation, reduced after-decay heat, etc. However, in order to apply W materials to higher power neutron source rotating solid targets and fusion reactor plasma facing materials and components, it is required to enhance fracture resistances to embrittlement by a high ductile-to-brittle transition temperature (low temperature embrittlement), by recrystallization and grain growth (recrystallization embrittlement) and by neutron and light ion irradiations (radiation embrittlement), which limits structural applications of the metal.

Nano-structures with dispersoids are very effective in mitigating the problems in W. The authors have developed ultra-fine grained (UFG) W–(0.25–1.5)wt.%TiC compacts with equiaxed grains of 50–200 nm in size and TiC dispersoids by utilizing mechanical alloying (MA) [2] in a purified H_2 or Ar atmosphere and hot isostatic pressing (HIP) processes [3–6]. The main features of UFG W–TiC/H_2 (MA atmosphere: H_2) or W–TiC/Ar (MA atmosphere: Ar) are:

(1) Microstructure: UFG W–TiC/Ar contains nano-sized Ar bubbles, which result in less densification, but contribute to grain refinement [5,6]. The grain size in W–TiC/Ar is about half of that in W–TiC/H_2. Increase in TiC addition leads to grain refinement. (2) Room-temperature mechanical properties: TiC addition significantly improves 3-point bend fracture strength from ~1.0 GPa in pure W to 1.5–2.0 GPa in (0.25–1.5)%TiC additions with less TiC dependence [7]. MA in a H_2 atmosphere results in higher fracture strength than that in Ar, however, even W–TiC/H_2 exhibits no appreciable ductility at room temperature [6,7]. (3) High temperature mechanical properties [7–10]. Above 1673 K UFG W–TiC compacts exhibit superplasticity. The elongation, flow stress and *m*-value (strain rate sensitivity of flow stress) depend strongly on TiC addition and MA atmosphere. TiC addition enhances the elongation and residual Ar decreases the elongation, flow stress and *m*-value. (4) Irradiation performance: neutron irradiation at 873 K to 2×10^{24} n/m^2 ($E_n > 1$ MeV) causes no hardening for UFG W–0.5TiC/Ar or W–0.5TiC/H_2 [6]. For 3 MeV He irradiation above 673 K UFG W–0.3TiC/H_2 exhibits high resistance to surface exfoliation mainly

* Corresponding author.
E-mail address: kurishi@imr.tohoku.ac.jp (H. Kurishita).

0022-3115/$ - see front matter © 2009 Elsevier B.V. All rights reserved.
doi:10.1016/j.jnucmat.2009.10.015

due to enhanced diffusion of implanted He in the nanostructure [6,7,11]. For 1 keV H (with 0.8%C) irradiation at 653 K W–0.5TiC/H_2 has a preferable feature for hydrogen blistering but shows many small holes [12].

The above indicates that the assurance of room-temperature ductility and enhancement of surface resistance to low-energy hydrogen irradiation remain unaccompanied for UFG W–TiC. The purpose of this study is to clarify the microstructural factors responsible for the problems and achieve microstructual modifications of UFG W–TiC to enhance room-temperature ductility and the resistances to radiation performance. It is shown that microstructural modification by hot plastic working allows us to convert UFG W–TiC/Ar and W–TiC/H_2 to *fine* grained compacts exhibiting appreciable RT-ductility by strengthening of grain boundaries in a re-crystallized state. It is also shown that the modified microstructures are highly resistant to low energy, high flux, high fluence ion bombardment at ~573 K in pure deuteron (D) and D + He mixture plasmas [13]. This method can also provide the possibility of improved resistances to recrystallization embrittlement.

2. Experimental

Powders of pure W (an average particle size 4.0 μm and purity 99.9%) and TiC (1.0 μm, 99.9%) were mixed to provide nominal compositions of W–0.6, 1.0, 1.1TiC (in wt.%) in a glove box filled with a purified Ar or H_2 gas (purity 99.99999%). Each of the powder mixtures was then charged into two vessels made of TZM (Mo–0.5Ti–0.1Zr) together with TZM balls for MA. The inner atmosphere of the vessels for MA was purified Ar or H_2 gas. MA treatments were conducted by a 3MPDA (three mutually perpendicular direction agitation) ball mill for 60–100 h. The details of the MA processes were reported elsewhere [3].

The MA processed powder was heated at 1073 K for 3.6 ks in a vacuum to remove the introduced Ar or H_2 gas during MA. The degassed powder was enclosed into a mild steel capsule and then subjected to HIP in an Ar atmosphere at 1620 K and 200 MPa for 10.8 ks. HIP at 1 GPa was also conducted at 1670 K for 7.2 or 10.8 ks at Japan Ultra-high Temperature Materials Research Institute (JUTEM). The dimensions of the as-HIPed compacts were approximately 25 mm in diameter and 26 mm in height. Hereafter, W–TiC compacts fabricated by MA in a purified H_2 or Ar atmosphere are called W–TiC/H_2 or W–TiC/Ar, respectively.

The as-HIPed compacts were subjected to compression forming at temperatures from 1873 to 2023 K in a vacuum better than 5×10^{-4} Pa with reduction ratios of 70–85%.

The compacts in the as-HIPed and compression formed states were machined to prepare miniaturized bend specimens with the dimensions of 1 mm by 1 mm by 10 or 20 mm, followed by mechanical polishing with emery disks up to #1500. The specimens were deformed by 3-point bend tests at room temperature and crosshead speed of 1×10^{-3} mm/s. Fracture surfaces were examined with a field emission scanning electron microscope (FE-SEM).

Thin foils for transmission electron microscopy (TEM) observations were prepared by twin-jet electropolishing using a solution of 20 vol.% H_2SO_4 and 80 vol.% C_2H_5OH around 278 K at 20 V. They were subjected to TEM examinations and EDX analyses using a JEM-2000FX operating at 200 kV.

3. Results and discussion

3.1. Determinant factors

In general, the assurance of RT-ductility requires to increase the fracture strength well above the yield strength. Fracture in UFG W–TiC occurs mainly at grain boundaries and most of the grain boundaries exhibit random orientations, the CSL (coincidence site lattice) grain boundaries being approximately 20% [14]. Thus, strengthening of such random weak grain boundaries is needed to increase the fracture strength.

As mentioned in the introduction, MA in H_2 results in higher fracture strength than that in Ar, and W–TiC/H_2 exhibits higher relative density and no observable bubbles. These results suggest that residual Ar bubbles or pores may be the determinant factor of fracture strength of UFG W–TiC. If this is the case, HIPing at higher pressures can lead to increase the fracture strength of the as-HIPed compacts, especially for W–TiC/Ar. In order to confirm this point, W–(0.6, 1.1)TiC/Ar and W–(0.6, 1.1)TiC/H_2 compacts were prepared for HIPing at 1 GPa and subjected to 3-point bend tests at room temperature. The 3-point bend test results are shown in Fig. 1 in comparison with those for HIPing at 0.2 GPa. The fracture strength was estimated to be the maximum fiber stress given by

$$\sigma = 3PL/2WB^2 \quad (1)$$

Here, σ is the stress, P is the applied load, L is the span, W and B are the specimen width and thickness, respectively. It should be noted that HIPing at 1 GPa does not increase the fracture strength of W–TiC/H_2, but significantly increases the fracture strength of W–TiC/Ar from 1.3 ~ 1.5 GPa (HIP at 0.2 GPa) to 2.0 GPa for W–0.6TiC/Ar and to 2.6 GPa for W–1.1TiC/Ar, which is considerably higher than the highest strength of ~2 GPa in W–(0–1.5)TiC/H_2. Residual Ar bubbles or pores are hence surely the determinant factor responsible for no RT-ductility.

Another factor responsible for no RT-ductility is very high yield strength of UFG W–TiC due to the Hall Petch effect because the fracture strength of 2.6 GPa for W–1.1TiC/Ar is still lower than the yield stress. Appropriate decrease in yield strength will contribute to enhance RT-ductility as well. The yield strength can be readily decreased by increasing grain size.

Low-energy hydrogen irradiation to UFG W–0.5TiC/H_2 caused many small holes, which were produced probably by ejection of ultra-fine grains [12]. This grain ejection can be attributed to weakening of grain boundaries intersecting with the specimen surface as a result of a high hydrogen concentration. The hydrogen concentration at grain boundaries will increase with decreasing grain size because the penetration depth of low-energy hydrogen is very limited and grain boundaries act as preferential hydrogen trapping

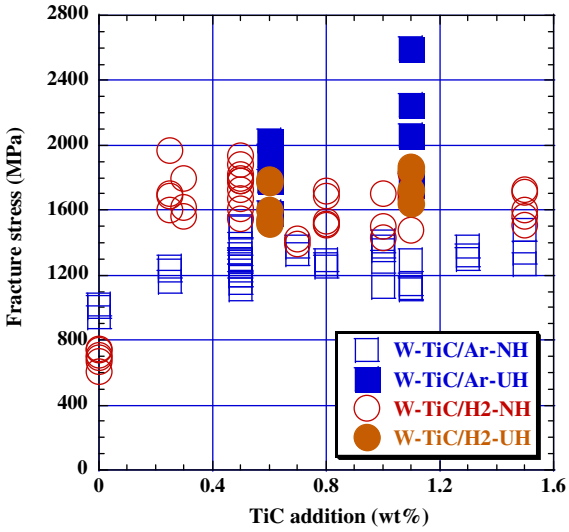

Fig. 1. Effects of HIPing pressure and MA atmosphere on 3-point bend fracture strength at room temperature for W–TiC/Ar and W–1TiC/H_2. UH stands for HIP at an ultra high pressure of 1 GPa and NH for HIP at 0.2 GPa.

sites. It is therefore considered that the determinant factors for resistance to low-energy hydrogen irradiation are grain boundary structure and grain size.

Increase in grain size usually takes place via a recrystallization process, which results in recrystallization embrittlement. Recrystallization embrittlement is well known to be caused by weakening of grain boundaries introduced during recrystallization, and it is required that the grain boundaries in a re-crystallized state are strengthened.

Therefore, the microstructural modification to be sought should meet the following requirements; strengthening of grain boundaries, a thorough removal of residual Ar bubbles and pores and adjustment of grain size to appropriate one.

3.2. Microstructural modification and 3-point bend test results

Hot plastic working is a process relevant to the microstructural modification. Superplasticity has been applied to W–(1.0–1.1)TiC/Ar and W–1.1TiC/H_2 to perform hot plastic working since UFG W–TiC is poorly deformable except for the superplastic condition. 1.0–1.1%TiC additions have been found to provide the highest elongation and relatively low flow resistance at 1773–1973 K among W–(0–1.5)TiC/Ar and W–(0–1.5)TiC/H_2 [7,10].

Hot compression forming processes have been used for plastic working. Fig. 2 shows effects of compression forming temperature and reduction ratio on the RT fracture strength of UFG W–1.0TiC/Ar HIPed at 0.2 GPa (W–1TiC/Ar-NH). The fracture strength significantly increases by compression forming and reaches a value as high as 3.5 GPa at 1923 K at reduction ratio around 80%. However, even in this case the amount of plastic deformation was very small because of a very high value of the proportionality limit (approximately 2.9 GPa) and large initial work hardening rate (see Fig. 3). Therefore, the UFG W–1.1TiC/Ar compact HIPed at 1 GPa (W–1.1TiC/Ar-UH), which showed much higher fracture strength than W–1.1TiC/Ar-NH (Fig. 1), has been subjected to compression forming at 1923 K to approximately 80% in reduction ratio. The results are shown in Fig. 2 together with the fracture strength of as-HIPed W–1.1TiC/Ar-UH. It should be noted that compression forming results in remarkable increase in RT fracture strength and the beneficial effects of compression forming vary with the fracture strength in the as-HIPed state. The RT fracture strength of compression formed W–1.1TiC/Ar-UH reaches a value as high as 4.4 GPa. To the best of the authors' knowledge, this RT fracture strength is the highest among the W materials reported so far.

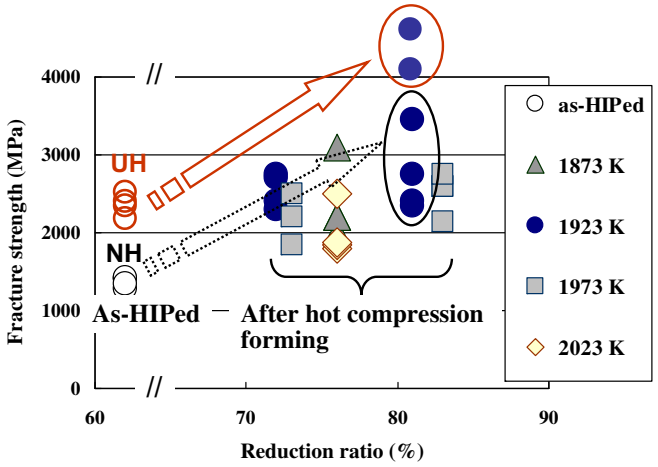

Fig. 2. Effects of compression forming temperature and reduction ratio on 3-point bend fracture strength at room temperature for W–(1.0–1.1)TiC/Ar. UH stands for HIP at an ultra high pressure of 1 GPa and NH HIP at 0.2 GPa.

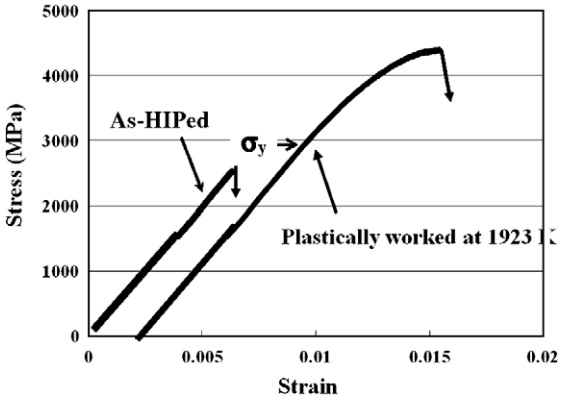

Fig. 3. The 3PB stress strain curves for W–1.1TiC/Ar-UH before and after compression forming to approximately 80% in reduction ratio at 1923 K. σ_y indicates the proportional limit (yield stress).

Fig. 3 shows 3-point bend stress strain curves for W–1.1TiC/Ar-UH before and after compression forming at 1923 K to approximately 80% in reduction ratio. Plastically worked W–1.1TiC/Ar-UH exhibits its yield and fracture stresses of 2.8 and 4.4 GPa, respectively, with a stress difference of 1.6 GPa, possessing appreciable RT-ductility. It is also recognized that fracture in compression formed W–1.1TiC/Ar-UH occurs fairly gradually in comparison with that in as-HIPed W–1.1TiC/Ar-UH, as suggested by the arrows in Fig. 3. This is also a favorable property.

On the other hand, W–1.1TiC/H_2 exhibits a larger grain size than W–1.1TiC/Ar and thus is expected to show lower yield stress and more appreciable ductility. W–1.1TiC/H_2 HIPed at 0.2 GPa (W–1.1TiC/H_2-NH) and 1.0 GPa (W–1.1TiC/H_2-UH) have been compression formed although HIPing at 1 GPa did not yield any strength increase for W–1.1TiC/H_2 compared with HIPing at 0.2 GPa (Fig. 2). Both materials after compression forming exhibited improved fracture resistance, however, the degree of the improvement was less in W–1.1TiC/H_2-UH than in W–1.1TiC/H_2-NH. The reason of the difference is not clear at present. Fig. 4 shows 3-point bend stress strain curves for W–1.1TiC/H_2-NH before and after compression forming at 1923 K to approximately 80% in reduction ratio. The yield and fracture stresses are approximately 2.2 and 3.3 GPa, respectively. A noted feature of compression formed W–1.1TiC/H_2 is that the work hardening rate after deviation from the initial linearity is much lower, namely RT-ductility is more noticeable in W–1.1TiC/H_2 than in W–1.1TiC/Ar-UH. This lower work

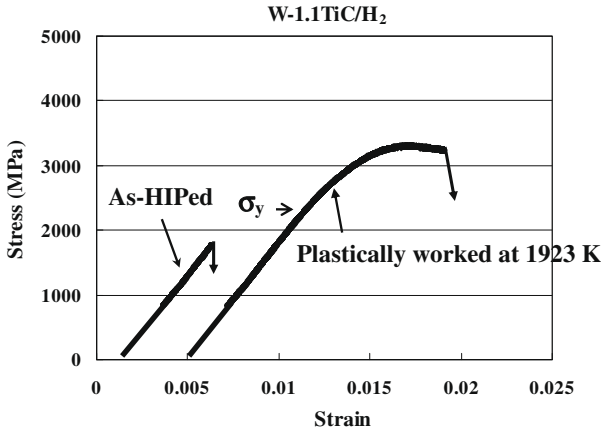

Fig. 4. The 3-point bend stress strain curves for W–1.1TiC/H_2-NH before and after compression forming to approximately 80% in reduction ratio at 1923 K. σ_y indicates the proportional limit (yield stress).

hardening rate can be associated with larger grain size and lower yield strength in W–1.1TiC/H_2 than in W–1.1TiC/Ar-UH. This indicates the significance of size of the grain interior in which plastic deformation occurs by dislocation multiplication and movements for the assurance of RT-ductility.

Fig. 5 shows fracture surfaces of 3-point bend tested specimens of W–1.1TiC/Ar-UH and W–1.1TiC/H_2-NH in the compression formed state. It appears that both specimens fractured not only by intergranularly, but also by transgranularly, the areas of transgranular fracture being marked by circles. This occurrence of transgranular fracture at such very high stresses indicates that a large number of grain boundaries are much strengthened by hot compression forming and exhibit superior boundary decohesion resistance. A low magnified micrograph of the same fracture surface in W–1.1TiC/Ar-UH is shown in Fig. 5(c). The fracture initiation site is marked by the arrow in the figure and fracture appears to originate from a stress concentrator like an inclusion. This implies that the intrinsic fracture strength of W–1.1TiC/Ar-UH without such stress concentrators should exceed the measured value of 4.4 GPa, providing evidence of the significant strengthening of grain boundaries by compression forming.

3.3. Density and microstructures

In order to elucidate the cause of remarkable enhancement of fracture resistance by compression forming, density measurements were conducted for the specimens before and after compression forming at 1923 K up to approximately 80% in reduction ratio. The result is shown in Table 1. The measured densities after compression forming are approximately equal to the theoretical density (100% relative density) of each material, suggesting thorough removal of nano-sized Ar bubbles and pores. The difference in the density after compression forming between W–1.1TiC/H_2-NH and W–1.1TiC/Ar-UH or W–1.0TiC/Ar-NH is mainly due to the content of Mo impurity introduced during MA from milling vessels and balls made of TZM; the Mo content in

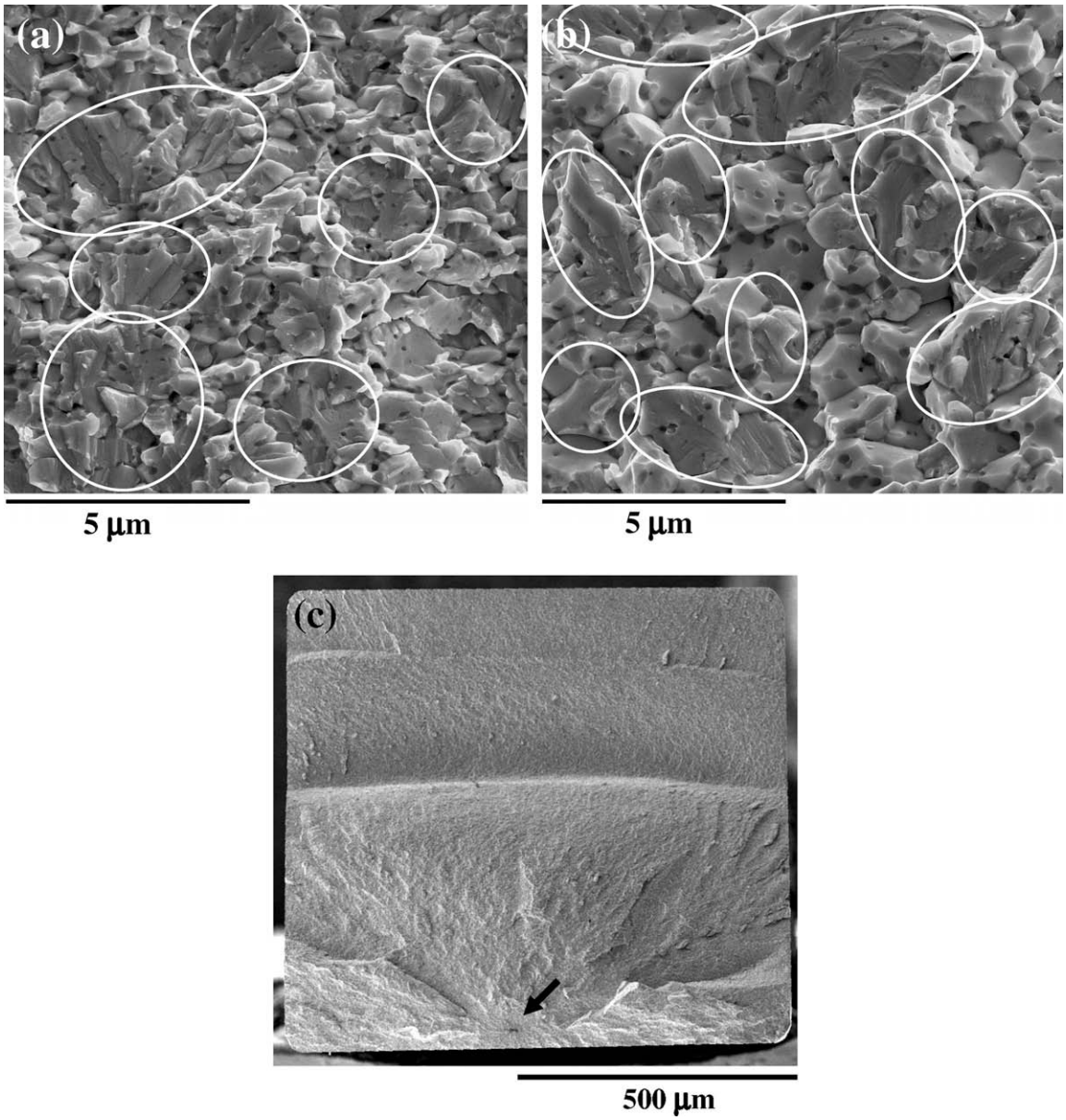

Fig. 5. SEM images of fracture surface of 3PB tested specimens of (a) and (c) W–1.1TiC/Ar-UH and (b) W–1.1TiC/H_2-NH after compression forming to approximately 80% in reduction ratio at 1923 K. The areas of transgranular fracture are marked by circles and the fracture initiation site is marked by the arrow.

Table 1
Designation, TiC addition, processing conditions and measured density of specimens used.

Designation	TiC addition (%)	MA atmosphere	HIPing pressure (GPa)	Compression forming temperature (K)	Measured density (g/cm^3)
W–1.0TiC/Ar-NH	1.0	Purified Ar	0.2	–	17.74
W–1.0TiC/Ar-NH	1.0	Purified Ar	0.2	1923	18.37
W–1.1TiC/Ar-UH	1.1	Purified Ar	1.0	–	18.39
W–1.1TiC/Ar-UH	1.1	Purified Ar	1.0	1923	18.39
W–1.1TiC/H_2-NH	1.1	Purified H_2	0.2	–	17.81
W–1.1TiC/H_2-NH	1.1	Purified H_2	0.2	1923	18.13

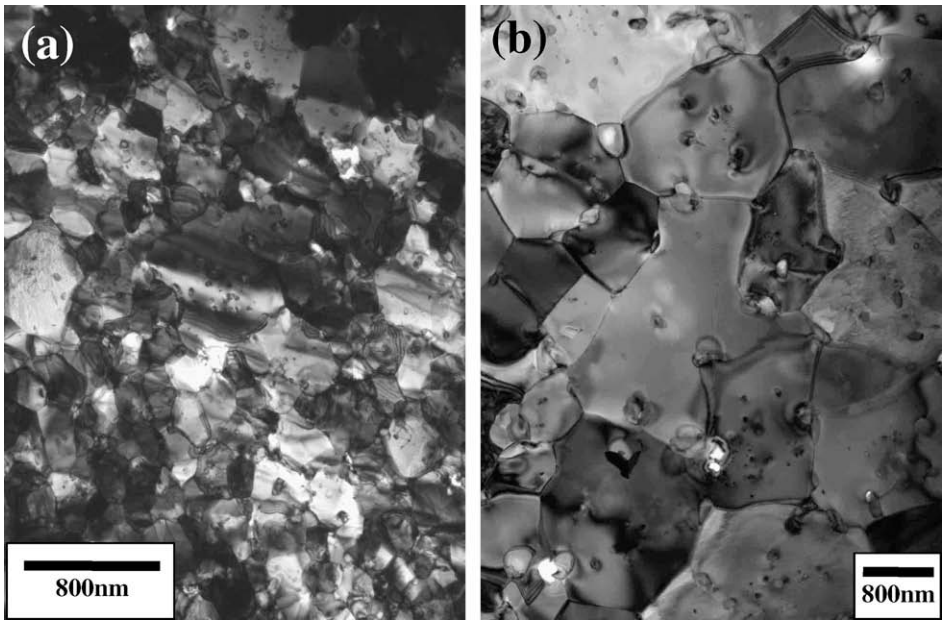

Fig. 6. TEM bright-field images showing grain structures for (a) W–1.1TiC/Ar-UH and (b) W–1.1TiC/H_2-NH after compression forming to 80% in reduction ratio at 1923 K.

W–1.1TiC/H_2-NH was higher than that in W–1.1TiC/Ar-UH and W–1.0TiC/Ar-NH.

It should be noted that the density of W–1.1TiC/Ar-UH remains constant irrespective of compression forming, 18.39 g/cm^3, which is approximately equal to the theoretical density of W–1.1TiC/Ar. In addition, compression formed W–1.0TiC/Ar-NH exhibits about the same density as compression formed W–1.1TiC/Ar-UH. These results indicate that the observed enhancement of fracture resistance cannot be explained by the effect of residual pores.

Figs. 6 and 7 show TEM bright-field images of microstructures and grain size distribution in W–1.1TiC/Ar-UH and W–1.1TiC/H_2-NH after compression forming to approximately 80% in reduction ratio at 1923 K. Recrystallization and grain growth occurred, with the average grain sizes of 520 and 1480 nm, which are approximately one order larger than those in the as-HIPed compacts of W–1.1TiC/Ar-UH and W–1.1TiC/H_2-NH, respectively. In general, an increase in grain size leads to decrease in fracture resistance, and in particular for group VIA transition metals such as W recrystallization and grain growth cause serious embrittlement. Nevertheless, as shown in Figs. 3 and 4 the fracture strength of both compacts is markedly increased. This enhancement of fracture resistance by compression forming can be attributed to significant strengthening of grain boundaries, which is in accordance with the results shown in Fig. 5. The observed difference of fracture resistance between compression formed W–1.1TiC/Ar-UH and W–1.0TiC/Ar-NH can be attributed to the difference in grain boundary strength, which depends on the microstructure in the as-HIPed state.

Such grain boundary strengthening may be attributed to increase in the amount of TiC dispersoids existing at grain boundaries and to changes in grain boundary structures from high-energy random orientations to low-energy CSL orientations. Determination of grain boundary character distribution for the compression formed specimens is now in progress by on-line and automated analysis with orientation imaging microscopy (OIM).

In this study, a very important processing technology based on superplastic deformation has been developed. Application of the technology allows us to significantly strengthen weak grain boundaries in a re-crystallized state, resulting in very high fracture strength and appreciable RT-ductility for W–1.1TiC/Ar and W–1.1TiC/H_2. This result implies enhancement in resistance to recrystallization embrittlement, which is the major concern with the application of group VIA transition metals.

3.4. Pure D and D + He mixture plasma exposure

Very recently, blister formation and D retention in W have been investigated for low energy ($\sim$55 ± 15 eV), high flux ($\sim 10^{22}$ m^{-2} s^{-1}), high fluence (4.5×10^{26} m^{-2}) ion bombardment at moderate temperature ($\sim$573 K) in pure D and mixed species D + 20%He plasmas in the linear divertor plasma simulator PISCES-A at the University of California, San Diego [13]. The W materials used are stress-relieved pure W (SR-W), re-crystallized pure W (RC-W) and the compression formed samples of W–1.1TiC/Ar-UH and W–1.1TiC/H_2-UH.

It has been found that W–1.1TiC/Ar-UH and W–1.1TiC/H_2-UH exhibit superior performance to SR-W and RC-W; no holes and no blisters are formed, and consequently D retention is much less than those in SR-W and RC-W of $\sim 10^{21}$ m^{-2} by around two orders of magnitude [13]. The observed superior properties of W–1.1TiC/

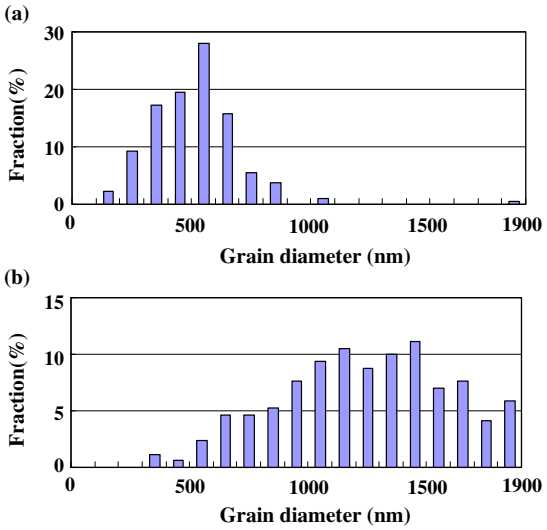

Fig. 7. Size distribution of grains in (a) W–1.1TiC/Ar-UH and (b) W–1.1TiC/H_2-NH after compression forming to 80% in reduction ratio at 1923 K.

Ar-UH and W–1.1TiC/H_2-UH can be attributed not only to their much finer grain size than that of SR-W and RC-W [13], but also to the modified microstructure where the grain boundaries are significantly strengthened in the re-crystallized state.

In addition, it is important to state the finding that addition of He to pure D (mixture of D and He) significantly suppresses blistering and D retention in the W materials [13]. This is most likely because the formation of nano-sized high density He bubbles in the near surface act as a diffusion barrier to implanted D atoms and consequently reduces the amount of uptake in the W material [13].

4. Conclusions

(1) Microstructural modifications to assure RT-ductility and improve resistance to grain ejection by low-energy hydrogen irradiation and re-crystallization embrittlement in the UFG W–TiC compacts should meet the following requirements; thorough removal of residual Ar bubbles and sintering pores, strengthening of grain boundaries and adjustment of grain size to appropriate one.

(2) Microstructural modification by hot plastic working based on superplasticity allows us to convert UFG W–1.1TiC/Ar and W–1.1TiC/H_2 to compacts exhibiting approximately theoretical density and high fracture resistance with a very high fracture strength and appreciable RT-ductility.

(3) W–1.1TiC/Ar HIPed at 1 GPa and hot plastically worked at 1923 K to 80% in reduction ratio exhibits a fracture strength of 4.4 GPa, which is the highest among the W materials reported so far. This is mainly due to strengthening of weak grain boundaries by microstructural modification. The degree of grain boundary strengthening depends on the microstructure in the as-HIPed state for the same TiC additions.

(4) RT-ductility in W–1.1TiC/H_2 is more noticeable than in W–1.1TiC/Ar. This is due to lower yield strength followed by lower work hardening rate, which can be attributed to larger grain size in W–1.1TiC/H_2.

(5) The microstructurally modified compacts of W–1.1TiC/Ar and W–1.1TiC/H_2 exhibit re-crystallized structures with grain sizes of approximately 0.5 and 1.5 μm, respectively. The grain boundaries in the re-crystallized state are much strengthened, and thus the compacts have been confirmed to exhibit improved resistance to surface exfoliation such as grain ejection and blistering by low-energy deuteron irradiation.

(6) The present processing technology based on superplastic deformation can provide the possibility of improved resistance to recrystallization embrittlement by producing significantly strengthened grain boundaries in the re-crystallized state.

Acknowledgments

The present work was supported by Grant-in-Aid for Scientific Research (B) (#19360412), Japan Society for the Promotion of Science (JSPS), which is greatly appreciated.

References

[1] For instance, G.S. Bauer, this Proceedings, 398 (2010) 19–27.
[2] J.S. Benjamin, Met. Trans. 5 (1970) 2943.
[3] Y. Ishijima, H. Kurishita, H. Arakawa, M. Hasegawa, Y. Hiraoka, T. Takida, K. Takebe, Mater. Trans. 46 (2005) 568–574.
[4] H. Kurishita, H. Arakawa, H. Matsui, Y. Amano, S. Kobayashi, K. Nakai, Y. Hiraoka, T. Takida, K. Takebe, J. Nucl. Mater. 367–370 (2007) 1453–1457.
[5] H. Kurishita, S. Kobayashi, K. Nakai, H. Arakawa, S. Matuso, T. Takida, K. Takebe, M. Kawai, Phys. Scr. T 128 (2007) 76–80.
[6] H. Kurishita, S. Kobayashi, K. Nakai, T. Ogawa, A. Hasegawa, K. Abe, H. Arakawa, S. Matsuo, T. Takida, K. Takebe, M. Kawai, N. Yoshida, J. Nucl. Mater. 377 (2008) 34–40.
[7] H. Kurishita, S. Matuso, H. Arakawa, H. Hirai, J. Linke, M. Kawai, N. Yoshida, Adv. Mater. Res. 59 (2009) 18–30.
[8] H. Kurishita, S. Matsuo, H. Arakawa, S. Kobayashi, K. Nakai, T. Takida, K. Takebe, M. Kawai, Mater. Sci. Eng. A 477 (2008) 162–167.
[9] S. Matsuo, H. Kurishita, H. Arakawa, T. Takida, M. Kato, Y. Yamamoto, K. Takebe, M. Kawai, N. Yoshida, Mater. Sci. Eng. A 492 (2008) 475–480.
[10] H. Kurishita, S. Matsuo, H. Arakawa, M. Narui, M. Yamazaki, T. Sakamoto, S. Kobayashi, K. Nakai, T. Takida, K. Takebe, M. Kawai, N. Yoshida, J. Nucl. Mater. 386–388 (2009) 579–582.
[11] T. Ogawa, A. Hasegawa, H. Kurishita, S. Nogami, J. Nucl. Sci. & Tech. 46 (2009) 717–723.
[12] Y. Ueda, N. Ohno, S. Kajita, H. Kurishita, H. Iwakiri, K. Tokunaga, N. Yoshida, Fusion Sci. Technol. 52 (2007) 513–520.
[13] M. Miyamoto, D. Nishijima, Y. Ueda, R.P. Doerner, H. Kurishita, M.J. Baldwin, S. Morito, K. Ono, J. Hanna: Nucl. Fusion 49 (2009) 065035.
[14] H. Kurishita, H. Arakawa, S. Matsuo, M. Kajioka, T. Sakamoto, S. Kobayashi, K. Nakai, V. Yardley, S. Tsurekawa, T. Takida, M. Kato, M. Kawai, N. Yoshida, J. Nucl. Mater., submitted for publication.